



MOF-derived Co/Zn single-atom catalysts for reversible hydrogenation and dehydrogenation of quinoline hydrogen carrier

Kanagaraj Naveen^a, Tahereh Mahvelati-Shamsabadi^a, Pragyan Sharma^a, Seong-hun Lee^{b,c},
Seung Hyun Hur^a, Won Mook Choi^{a,*}, Tae Joo Shin^{b,c,**}, Jin Suk Chung^{a,*}

^a School of Chemical Engineering, University of Ulsan, 93 Daehak-ro, Nam-Gu, Ulsan 44610, Republic of Korea

^b Unist Central facilities, Ulsan National Institute of Science and Technology (UNIST), 50 Unist-gil, Ulsan 44919, Republic of Korea

^c Graduate School of Semiconductor Materials and Devices Engineering, Ulsan National Institute of Science and Technology (UNIST), 50 Unist-gil, Ulsan 44919, Republic of Korea

ARTICLE INFO

Keywords:

Single-atom catalysts
Liquid organic hydrogen carrier
Quinolines derivatives
Reversible hydrogenation/dehydrogenation
Non-precious metal catalysts

ABSTRACT

Storage of hydrogen, particularly liquid organic hydrogen carrier (LOHC), has attracted much attention to address the problem of safe storage and transport of H₂. N-heterocycles are promising hydrogen carriers for storing/releasing hydrogen through reversible catalytic hydrogenation/dehydrogenation cycles. Therefore, designing cost-effective, efficient, reusable single catalysts for both processes with high catalytic activity is currently of interest. Herein, we report the successful preparation of atomically dispersed Co/Zn single-atom catalysts on nitrogen-doped carbon by pyrolysis of bimetallic Co_xZn_y-MOF-508@Melamine. The synthesized Co_xZn_y-NC catalyst showed highly efficient catalytic activity for the reversible hydrogenation and dehydrogenation of quinoline derivatives in the same solvent. Catalytic reversible hydrogen storage/release was demonstrated for three consecutive cycles without losing efficiency. The main features of this work require low loading of catalysts compared to reported heterogeneous non-precious metal catalysts. A control experiment revealed that free N-H groups/N-atoms are essential for dehydrogenation/hydrogenation reactions, and a possible reaction mechanism was proposed.

1. Introduction

Due to the rapid depletion of fossil-based resources, global warming, environmental issues, and ever-increasing energy demand, the development of cost-effective, efficient, sustainable, and renewable energy conversion and storage systems have gained much attention. Hydrogen is considered an ideal alternative future energy carrier to replace fossil fuels because it is green, non-toxic, eco-friendly fuel, renewable, has no CO_x emissions, and has high energy density [1–3]. However, its safe and efficient storage and transportation remain a significant challenge for developing a hydrogen economy [4–6]. In this respect, storing hydrogen in the form of liquid organic hydrogen carriers (LOHCs) is a highly desirable method because of its safety, easy transport at room temperature and atmospheric pressure, and practical reusability to store and release hydrogen through reversible catalytic hydrogenation and dehydrogenation reactions [7–11]. Various LOHC compounds have been studied for hydrogen storage in the literature. However, storage

based on N-heterocycle LOHC systems is more attractive because the nitrogen atom in the ring can lower the dehydrogenation reaction temperature compared to cycloalkanes [12–14]. Therefore, designing efficient, cost-effective, reusable catalysts for hydrogen storage reactions with high catalytic activity and selectivity is of current interest [15,16].

In the past decade, various homogeneous and heterogeneous metal catalysts have been reported to perform either hydrogenation or dehydrogenation of N-heterocycles [17–22]. A few catalysts have been investigated to catalyze both reactions in different solvent systems [23–26]. However, reports of single catalysts based on precious metals for the acceptor-less reversible hydrogenation/dehydrogenation of N-heterocycles, especially quinoline derivatives, have been explored [27–31]. Notably, non-precious heterogeneous metal catalysts are more attractive in large-scale hydrogen storage applications due to their abundance, cost-effectiveness, separation of catalyst, and reusability, compared to the precious homo-/heterogeneous catalysts. Only three

* Corresponding authors.

** Corresponding author at: Unist Central facilities, Ulsan National Institute of Science and Technology (UNIST), 50 Unist-gil, Ulsan 44919, Republic of Korea.

E-mail addresses: wmchoi98@ulsan.ac.kr (W.M. Choi), tjshin@unist.ac.kr (T.J. Shin), jschung@mail.ulsan.ac.kr (J.S. Chung).

<https://doi.org/10.1016/j.apcatb.2023.122482>

Received 11 November 2022; Received in revised form 20 January 2023; Accepted 16 February 2023

Available online 24 February 2023

0926-3373/© 2023 Elsevier B.V. All rights reserved.

non-precious heterogeneous metal catalysts are currently known in the literature [32–34]. In 2011, Kaneda et al. reported that Cu nanoparticles supported TiO_2 as the first catalyst for reversible dehydrogenation/hydrogenation of quinoline derivatives. In this case, the reaction requires high catalyst loading (20 mol%) and pre-activation of the catalyst by additional H_2 . Beller et al. developed an intermetallic nickel silicide supported on fumed silica that catalyzes the same hydrogenation/dehydrogenation of N-heterocycles. However, this catalyst system still suffers from the high pressure (50 bar H_2) required in hydrogenation and the long reaction time (48 h) for dehydrogenation reaction with a high loading of catalyst (20 mol%). Later, Co nanoparticles supported on nitrogen-doped carbon were further explored by Li et al. In this study, the hydrogenation reaction was carried out at 10 mol% catalysts, and the reverse reaction required a high catalyst loading (50 mol%) and a long reaction time (48 h) with an additional 30 bar of argon atmosphere for 95% conversion. To overcome the drawbacks mentioned above, developing efficient, robust, reusable, and low-loading non-precious metal catalytic systems is highly desirable for the reversible dehydrogenation and hydrogenation of N-heterocycles under mild conditions.

In recent years, single-atom catalysts (SACs) consisting of atomically dispersed metal atoms on nitrogen-doped carbon supports have emerged as a promising new frontier in the field of catalysis, and they have become the subject of much active research [35–38]. SACs combine the advantages of both homogeneous and heterogeneous catalysts, such as the utilization of maximum active metal sites, high catalytic efficiency and selectivity, easy separation and recycling, and high stability under reaction conditions. However, preparing stable SACs without particle aggregation during synthesis or subsequent catalysis conditions remains a significant challenge [39]. Among the various synthetic methods for SACs, pyrolyzing metal-organic framework (MOF) to synthesis MOF-derived carbon materials can be used as excellent support to anchor SACs with high metal content and stability [40–42]. MOFs have emerged as a new type of porous materials constructed by homogeneously distributed metal ions/clusters coordinated by organic linkers, and have attracted incredible attention due to their tunable synthesis and diverse post-synthetic modification option as they usually retain their parent precursors morphology [43] and widely used as heterogeneous catalyst for various organic transformations [44–48]. Recently, interest has expanded to use MOF as sacrificial precursors or templates to prepare MOF-derived SACs. Due to the unique features of high surface areas, ordered porous structure, and doped nitrogen atoms, a simple pyrolysis process provides perfect support for dispersing and stabilizing SACs by forming strong metal-nitrogen coordination bonds [49]. Currently, the most frequently used MOF precursors for synthesizing MOF-derived SACs on nitrogen-doped carbon materials are limited to Zn-based bimetallic zeolitic imidazolate frameworks (ZIFs) [50]. However, the use of other MOFs to prepare SACs has rarely been reported in the literature [51–54]. Therefore, it is highly desirable to find new MOF precursors for anchoring isolated metal single-atoms with hierarchical porous structures, a subject still open for further research and development. In recent years, many precious and non-precious metal SACs have been prepared and demonstrated to exhibit excellent catalytic performance in electrocatalysis [35,36] and photocatalysis reactions [38]. Recent literature has reported that various supported SACs have efficient catalytic activity for various organic transformations [37]. Among these Co-SACs have attracted much attention due to their cheap, earth-abundant metal and efficiently catalyzed different reactions such as fluorination of acyl chlorides, aerobic oxidation of ethylbenzene, hydrogenation of nitroarenes and quinolines, selective dehydrogenation of formic acid [55–59]. To the best of our knowledge, the use of SACs for consecutive acceptor-less, reversible hydrogenation/dehydrogenation of LOHC in the same solvent medium has not been investigated.

Herein, we report the successful preparation of atomically dispersed non-precious metal Co/Zn single-atom active sites anchored on porous nitrogen-doped carbon by one-step pyrolysis of bimetallic $\text{Co}_x\text{Zn}_y\text{-MOF}$ -

508@Melamine. The obtained $\text{Co}_x\text{Zn}_y\text{-NC}$ catalyst exhibited excellent catalytic activity for acceptor-less, reversible hydrogenation and dehydrogenation of quinoline derivatives. The highlights of the designed Co/Zn SACs perform three consecutive cycles of hydrogen storage/release without loss of catalytic efficiency with a low catalyst loading (3 mol%). The vital features of the catalyst do not tend to aggregate under presented reaction conditions, which ensures that the nitrogen atoms-doped carbon structure efficiently stabilizes the anchored metal single-atoms.

2. Experimental

Materials and characterization details are given in the [supplementary data](#).

2.1. Preparation of $\text{Co}_x\text{Zn}_y\text{-MOF-508@Melamine}$

A mixture of terephthalic acid (5.0 mmol) and 4,4'-bipyridine (2.5 mmol) was dissolved in 40 mL of DMF at 120 °C for 5 min. Next, a dissolved solution of $\text{Co}(\text{NO}_3)_2 \cdot 6\text{H}_2\text{O}$ ($\text{Co}_x = 0.075$ mmol, 0.150 mmol, 0.225 mmol, and 1.0 mmol) and $\text{Zn}(\text{NO}_3)_2 \cdot 6\text{H}_2\text{O}$ ($\text{Zn}_y = 4.925$ mmol, 4.85 mmol, 4.775 mmol, and 4.0 mmol) in 35 mL of DMF was added to the above solution under an argon atmosphere. The resulting mixture was refluxed at 120 °C for 5 h (a pale pink color precipitate formed in 30–40 min of reaction). Then, 3.0 g of melamine was added, followed by the addition of 30 mL of DMF, and the resulting slurry was again stirred at 120 °C for 1 h. After slow solvent evaporation at 110 °C for 16–20 h, a pale pink solid was obtained and dried in a vacuum oven at 100 °C for 24 h.

$\text{Zn}_{5.0}\text{-MOF-508@Melamine}$ was synthesized in the same way without the addition of $\text{Co}(\text{NO}_3)_2 \cdot 6\text{H}_2\text{O}$, instead using 5.0 mmol of $\text{Zn}(\text{NO}_3)_2 \cdot 6\text{H}_2\text{O}$.

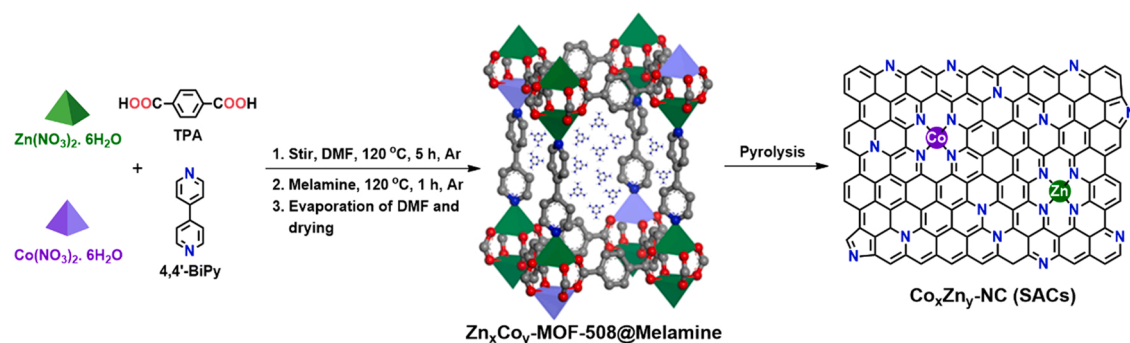
TPA:BPY@Melamine was synthesized without the addition of $\text{Co}(\text{NO}_3)_2 \cdot 6\text{H}_2\text{O}$ and $\text{Zn}(\text{NO}_3)_2 \cdot 6\text{H}_2\text{O}$.

2.2. Preparation of $\text{Co}_x\text{Zn}_y\text{-NC}$, Co(Np)-NC , $\text{Zn}_{5.0}\text{-NC}$ and NC

First, the solid material was ground to a fine powder, transferred to a ceramic boat, and placed in a tube furnace. Then, the furnace was purged with argon for 30 min, heated to 550 °C (5°C min^{-1}), and kept at 550 °C for 1 h under a flow of argon (6 cc min^{-1}). The temperature was further increased to 950 °C (5°C min^{-1}) and held at 950 °C for 3 h, and then it was naturally cooled to room temperature. Finally, pyrolyzed products such as $\text{Co}_{0.075}\text{Zn}_{4.925}\text{-NC}$, $\text{Co}_{0.15}\text{Zn}_{4.85}\text{-NC}$, $\text{Co}_{0.225}\text{Zn}_{4.775}\text{-NC}$, Co(Np)-NC , $\text{Zn}_{5.0}\text{-NC}$, and NC were used directly without any post-treatment (The values in the subscript stated that the corresponding mmole of cobalt and zinc precursors have been used in the preparation of MOFs for the synthesis of single-atom catalysts).

2.3. General procedure for the catalytic hydrogenation of quinoline derivatives

All reactions were performed using a 100 mL stainless-steel autoclave reactor charged with 3 mol% of $\text{Co}_{0.15}\text{Zn}_{4.85}\text{-NC}$ (37.7 mg), 0.5 mmol of substituted-quinolines (1a-e) and 3 mL of *i*-PrOH: H_2O (2:1). The reactor was sealed, purged three times with H_2 gas (4 bar) and pressurized to 6 bar H_2 . Then, the reaction temperature was raised to 110 °C for 20 min and stirred at 110 °C for 16 h. After completion of the reaction, the autoclave was cooled to room temperature in an ice bath, and the remaining H_2 gas was carefully released. The crude reaction mixture was diluted with chloroform, followed by filtration of the catalyst using a syringe filter and the reaction mixture was analyzed by GC. Conversions for each reaction were determined from the corresponding GC peak area integrations of products and reactants. The crude materials were purified by column chromatography.



Scheme 1. Schematic illustration for the synthesis of Co_xZn_y-NC.

2.4. General procedure for the catalytic acceptor-less dehydrogenation of tetrahydroquinoline derivatives

All reactions were performed using a 100 mL stainless-steel autoclave reactor charged with 3 mol% of Co_{0.15}Zn_{4.85}-NC (37.7 mg), 0.5 mmol of substituted-tetrahydroquinolines (2a-e), and 3 mL of *i*-PrOH:H₂O (2:1). Then, the reactor was sealed, purged three times with argon gas (10 bar), followed by heating to 200 °C for 40 min. The reaction mixture was stirred for 20 h. After the reaction time, the reactor was cooled to room temperature in an ice bath. The crude reaction mixture was diluted with chloroform, followed by filtration of the catalyst using a syringe filter and the reaction mixture was analyzed by GC. Conversions for each reaction were determined from the corresponding GC peak area integrations of products and reactants. The pure product was isolated by column chromatography.

2.5. Reversible hydrogenation/dehydrogenation between 1a and 2a

A 100 mL stainless-steel autoclave reactor was loaded with 3 mol% of Co_{0.15}Zn_{4.85}-NC (37.7 mg), 0.5 mmol of quinaldine 1a, and 3 mL of *i*-PrOH:H₂O (2:1). The autoclave was sealed and purged with H₂ gas (4 bar) three times and then pressurized to 6 bar H₂. The reaction mixture was heated to 110 °C for 20 min, followed by stirring at 110 °C for 16 h. The reactor was then cooled to room temperature in an ice bath and the remaining hydrogen was discharged. The conversion was determined by GC analysis of the crude reaction mixture. The same reaction mixture in the autoclave was sealed and purged three times with argon gas (10 bar) for the dehydrogenation reaction and was heated to 200 °C for 40 min. Then, the reaction mixture was stirred for 20 h and the reactor was cooled to room temperature in an ice bath. The conversion was determined by GC analysis of the crude reaction mixture. Next, another two cycles of successive hydrogenation/dehydrogenation reactions were performed with the same procedure. After 3 cycles, the catalyst was separated by centrifugation, washed with ethyl acetate and acetone, and dried at 60 °C overnight. Finally, the recycled catalyst was characterized.

2.6. Solvent-free hydrogenation of 1a

A mixture of 3 mol% of Co_{0.15}Zn_{4.85}-NC (378 mg) and 5.0 mmol of quinaldine 1a was added to a 100 mL stainless-steel autoclave reactor. The autoclave was sealed and purged with H₂ gas (4 bar) three times and then pressurized to 10–20 bar H₂. The reaction mixture was heated to 110 °C for 20 min, followed by stirring at 110 °C for 24 h. Then, the reactor was cooled to room temperature in an ice bath, and the remaining hydrogen was discharged. The reaction mixture was diluted with chloroform, followed by filtration of the catalyst using a syringe filter, and the conversion was determined by GC analysis of the crude reaction mixture.

2.7. Solvent-free dehydrogenation of 2a

A mixture of 3 mol% of Co_{0.15}Zn_{4.85}-NC (378 mg) and 5.0 mmol of 1,2,3,4-tetrahydroquinoline 2a was added into a 100 mL stainless-steel autoclave reactor. Then, the reactor was sealed, purged three times with argon gas (10 bar), and then heated to 200 °C for 40 min. The reaction mixture was stirred for 24–48 h. Then, the reactor was cooled to room temperature in an ice bath. The reaction mixture was diluted with chloroform, followed by filtration of the catalyst using a syringe filter, and then conversion was determined by GC analysis of the crude reaction mixture.

3. Result and discussion

3.1. Catalyst preparation and characterization

In this work, we successfully prepared a bimetallic Co/Zn metal-organic framework (Co/Zn-MOF-508) by a mixed-metal approach. The introduced cobalt metal partially replaced the zinc metal in the paddle-wheel bimetallic zinc carboxylate unit and reconstructed the paddle-wheel node structure by a mixed metal with ligands terephthalic acid (TPA) and pillared 4,4'-bipyridine (4,4'-BiPy) to form a 3D bimetallic Co/Zn metal-organic framework. The structure and morphology of the as-synthesized bimetallic MOF were characterized by powder X-ray diffraction (PXRD) analysis and scanning electron microscopy (SEM). As shown in Fig. S1, the presented XRD result confirmed that the mixed metal (Co/Zn-MOF-508) had the same patterns as Zn-MOF-508, which agreed well with previously reported literature [60]. The characteristic peaks indicate that the structure is not destroyed and establishes an identical structure with good crystallinity. In Fig. S2, SEM images show that both MOFs have similar morphologies of microrod structures [61]. Further, the synthesized MOFs were characterized by FT-IR and Raman spectroscopy (Figs. S3–S4).

Scheme 1 provides a schematic representation for the synthesis of Co_xZn_y-NC by pyrolysis of Co_xZn_y-MOF-508@Melamine. Initially, a bimetallic Co/Zn metal-organic framework was synthesized by refluxing Co(NO₃)₂·6H₂O, Zn(NO₃)₂·6H₂O in terephthalic acid and 4,4'-bipyridine in DMF at 120 °C for 5 h under Ar, forming a pale pink solid. To this MOF, melamine was added, and the whole reaction mixture was again stirred under the same condition for an additional 1 h. After slow DMF evaporation and drying in a vacuum oven, a CoZn-MOF-508@Melamine slurry was obtained as a pale pink powder. Then, the powder material was pyrolyzed at 550 °C for 1 h and 950 °C for 3 h under flowing argon, leading to Co and Zn metal anchored on a nitrogen-doped carbon material referred to as Co_xZn_y-NC. A series of catalysts, i.e., Co_{0.075}Zn_{4.925}-NC, Co_{0.15}Zn_{4.85}-NC, Co_{0.225}Zn_{4.775}-NC, and Co(Np)-NC were synthesized by pyrolysis of different Co_xZn_y-MOF-508@Melamine, obtained by tuning the moles of Co_(x) and Zn_(y) precursors in the preparation. To compare catalytic activity, we also prepared a Zn_{5.0}-NC catalyst by the same procedure to demonstrate its role in catalysis. The organic linkers (TPA and 4,4'-BiPy) were carbonized during pyrolysis processes, and the

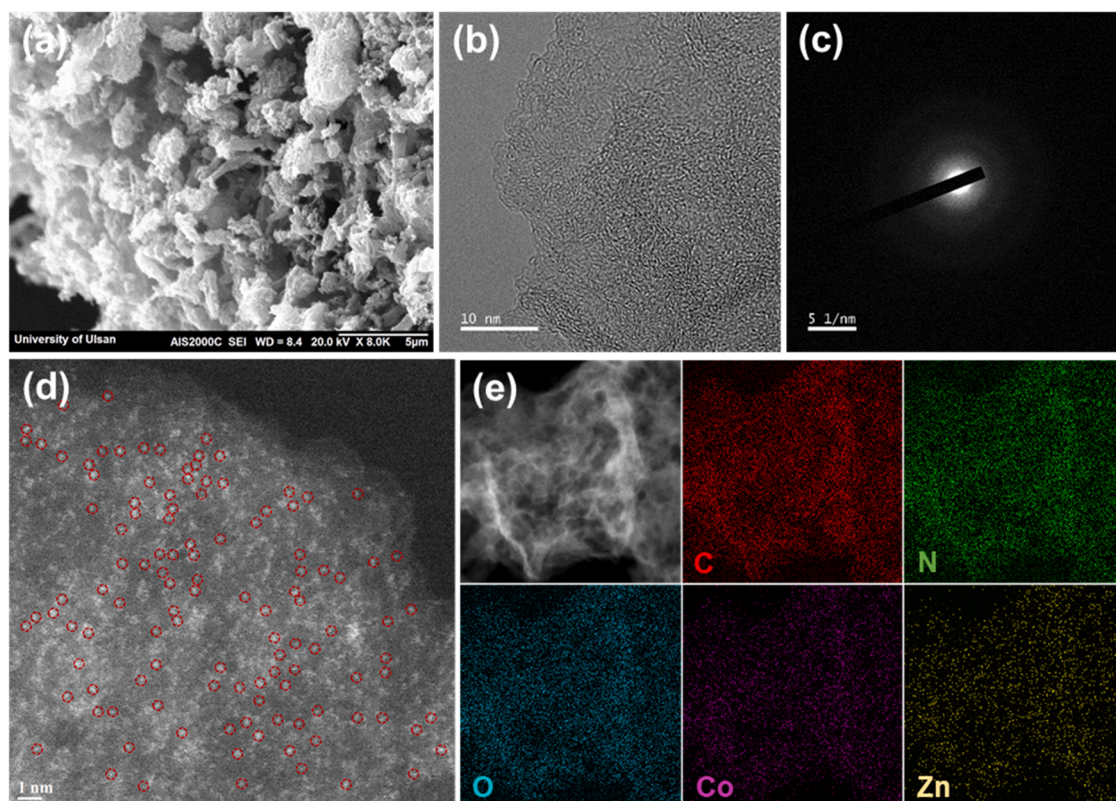


Fig. 1. Characterization of $\text{Co}_{0.15}\text{Zn}_{4.85}\text{-NC}$. (a) SEM image, (b) HR-TEM image, and (c) SAED pattern of $\text{Co}_{0.15}\text{Zn}_{4.85}\text{-NC}$. (d) Aberration corrected HAADF-STEM image of $\text{Co}_{0.15}\text{Zn}_{4.85}\text{-NC}$, scale bar is 1 nm (metal single atoms are marked by red circles). (e) HAADF-STEM image with corresponding EDS mapping of $\text{Co}_{0.15}\text{Zn}_{4.85}\text{-NC}$, scale bar is 50 nm.

melamine polymerized to form graphitic carbon nitride in the interstices of the carbon skeleton when held at 550°C , whereas the metal NPs were confined between the layers. As the pyrolysis temperature increased from 550°C to 950°C , the decomposition of carbon nitride created free N-rich sites with a carbon framework. At the same time, most of the Zn atoms were evaporated and the residual metal atoms (Co/Zn) were coordinated with N-sites in the carbon support, which prevented metal atom aggregation. The contents of Co and Zn in all samples were determined by inductively coupled plasma-optical emission spectrometry (ICP-OES) and elemental analysis was performed to evaluate the contents of C, N, O and H (Table S1).

First, the morphology and structure of the catalysts were characterized by scanning electron microscopy (SEM), transmission electron microscopy (TEM), and high-angle annular dark-field scanning transmission electron microscopy (HAADF-STEM). In Fig. 1a, the SEM image of the pyrolysis product $\text{Co}_{0.15}\text{Zn}_{4.85}\text{-NC}$ shows an irregular aggregate structure morphology that slightly retains the shape of the MOF, indicating the transformation into a carbon skeleton during pyrolysis. A high-resolution TEM image of $\text{Co}_{0.15}\text{Zn}_{4.85}\text{-NC}$ shows the absence of obvious metal nanoparticles in the graphitic carbon structure (Fig. 1b). The ring-like selected area electron diffraction (SAED) pattern of $\text{Co}_{0.15}\text{Zn}_{4.85}\text{-NC}$ demonstrated its poor crystallinity, implying there are no crystalline nanoparticles in the pyrolysis product (Fig. 1c). These results clearly suggest that the metals must be highly dispersed as single-atoms or tiny clusters on the carbon support. Aberration-corrected HAADF-STEM measurements were performed to confirm further the existential form of Co and Zn atoms (Fig. 1d). As shown in Fig. 1d, many isolated bright dots were uniformly distributed in the carbon structure of $\text{Co}_{0.15}\text{Zn}_{4.85}\text{-NC}$, which is attributed to the heavy metal atoms of Co and Zn. Further, the HAADF-STEM image and the corresponding elemental mapping images indicate that C, N, O, Co and Zn elements are homogeneously dispersed throughout the structures (Fig. 1e). As displayed in

Figs. S5–S7, other samples such as $\text{Co}_{0.075}\text{Zn}_{4.925}\text{-NC}$, $\text{Co}_{0.225}\text{Zn}_{4.775}\text{-NC}$, and $\text{Zn}_{5.0}\text{-NC}$ were similarly characterized. All of them showed a similar morphology as $\text{Co}_{0.15}\text{Zn}_{4.85}\text{-NC}$ and confirmed the atomic dispersion of metal atoms in the nitrogen-doped carbon structure without agglomeration.

Furthermore, the phase composition of the prepared catalysts was characterized by X-ray diffraction (XRD), with broad peaks at $\sim 25^\circ$ and $\sim 42^\circ$ attributed to the (002) and (101) planes of amorphous graphitic carbon, respectively (Fig. 2a). Moreover, no diffraction peaks related to the cobalt- or zinc-based species were detected in the XRD patterns, in good agreement with the HR-TEM and HAADF-STEM results, illustrating that metal atoms can be isolated in the form of single atoms. In Fig. S8, the XRD of Co(Np)-NC showed several peaks characteristic of forming face-centered cubic metallic Co crystals [57]. Raman spectra were recorded to investigate the degree of graphitization of the catalysts, which showed two peaks corresponding to the D band ($\sim 1331\text{ cm}^{-1}$) and G band ($\sim 1570\text{ cm}^{-1}$), respectively, and the intensity ratio of I_D/I_G was between 1.02 and 1.10 (Fig. 2b). In addition, the appearance of a broad 2D peak around $\sim 2860\text{ cm}^{-1}$ confirmed the presence of layered or graphitized structures of disordered carbon. The surface area and pore size distribution of prepared catalysts were analyzed by N_2 adsorption-desorption isotherms, as shown in Table S2. The isotherms for all $\text{Co}_x\text{Zn}_y\text{-NC}$ showed characteristics of type IV with hysteresis loops in the P/P_0 range of 0.4–1.0, indicating the presence of mesoporous structure (Fig. S9). The pore size distribution curve revealed that all catalysts have an abundant micro/mesoporous structure in the range of 0–20 nm (Fig. S10). These results indicate that the hierarchically porous structures of $\text{Co}_x\text{Zn}_y\text{-NC}$ catalysts expose more single-atom active sites and facilitate the mass transport of reactants/products during the reaction. The composition and chemical state of pyrolyzed materials were further investigated by X-ray photoelectron spectroscopy (XPS). The survey spectra of all samples revealed the presence of C, N, O, Co, and Zn

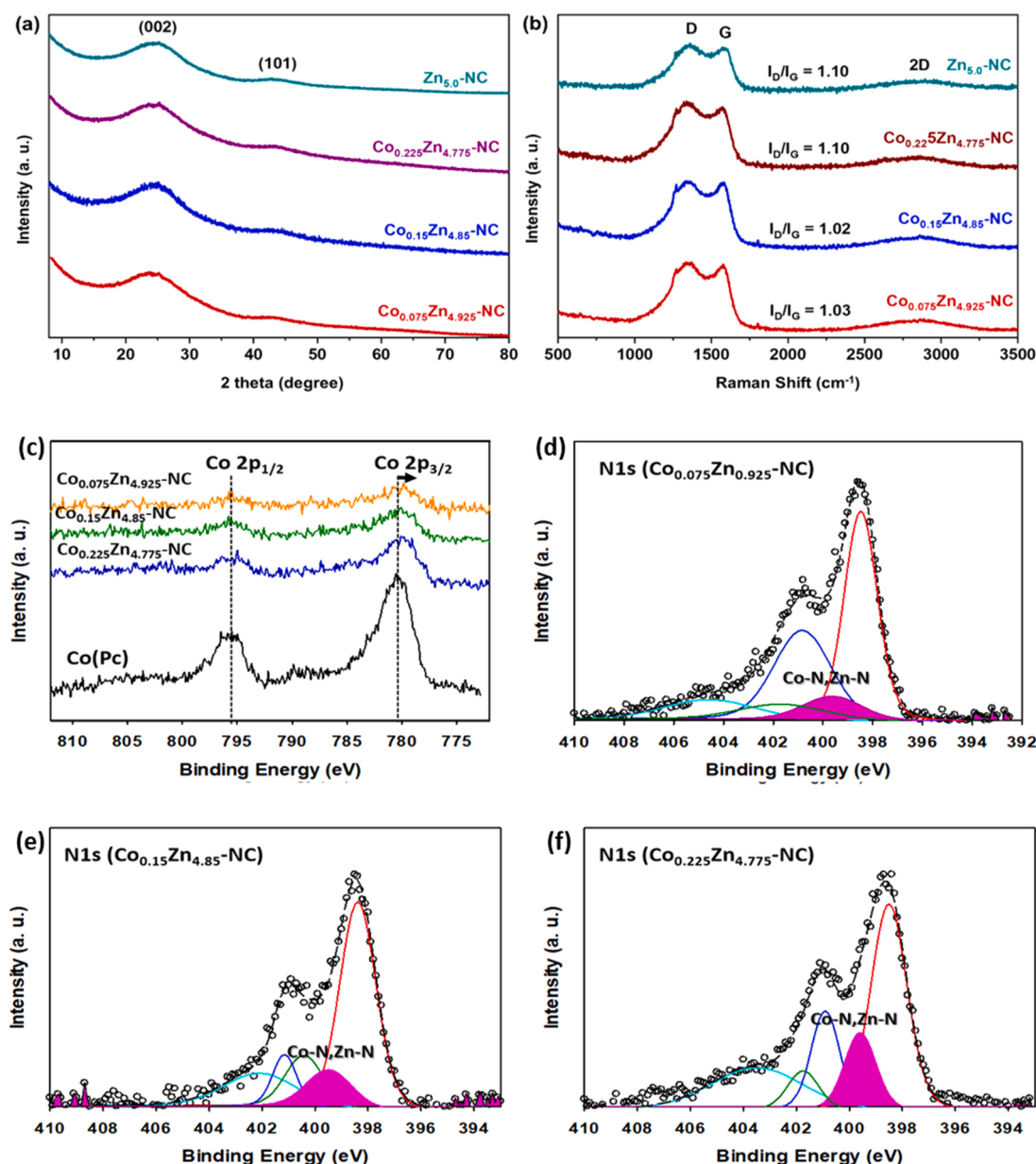


Fig. 2. (a) XRD patterns and (b) Raman spectra of Co_xZn_y-NC and Zn_{5.0}-NC. (c) High-resolution Co 2p spectra of Co_xZn_y-NC. (d-f) High-resolution N 1s spectra of Co_xZn_y-NC.

elements on the surface of the catalysts, which is consistent with the EDS elemental maps (Fig. S11). As shown in Figs. S12-S13, the high-resolution C 1s spectra of pyrolyzed products were deconvoluted into four peaks assigned to C-C/C=C (284.7 eV), C=N/C-O (285.6 eV), C=O/C-N (286.9 eV) and O-C=O (290.1 eV), respectively [62]. The O 1s XPS spectra were fitted as two peaks at 531.4 eV for C=O and ~532.8 eV for C-O, confirming that N and O atoms doped with the carbon skeleton [63]. The high-resolution Co 2p XPS spectrum showed two major peaks at ~780.0 and ~795.7 eV in all samples, assigned to Co 2p_{3/2} and Co 2p_{1/2}, (Fig. 2c), and belonging to the oxidation state of + 2 of cobalt (at almost the same position of cobalt in Co(Pc) with a small negative shift to the lower energy bands, Fig. 2c, which can be related to the less populated coordination environment of Co centers). The shoulder peak at around 785.0 eV which is more obvious for the sample with the highest cobalt amount is assigned to the Co satellite peak. Satellite peaks are used to identify shake-ups, energy loss, plasmons, and various unidentified peaks. These appear as peaks to the high binding energy sides to the main peak in the XPS [64,65]. Notably, the Co 2p

spectrum indicates no characteristic peak of metallic Co (at ~778.5 eV) [66]. The N 1s XPS spectra can be deconvoluted into five peaks, which are assigned to the N-pyridinic (398.5 eV), metal-nitrogen (M-N) at around 399.5 eV, pyrrolic (400.0 eV), N-graphitic (401.2 eV), and N-oxide (404.4 eV) (Fig. 2d-f) [67]. The N1s XPS spectrum of Co(Pc) could be deconvoluted into two peaks of pyridinic N (398.5 eV) and Co-N at around 399.3 eV (Fig. S14). Based on N1s spectra for the samples including Co_xZn_y-NC, Fig. 2d-f, and Zn_{5.0}-NC, Fig. S14, it is important to note that the new nitrogen peak emerges at around 399.5 eV in the spectrum which is assigned to the chemical bond of metal-N (Zn-N or Co-N or both) appears at almost the same position with Co-N peaks at around 399.3 eV in Co (Pc) (Fig. S14). In the Zn 2p XPS spectra of the pyrolysis products, two peaks located at binding energies of 1021.8 eV and 1044.8 eV were assigned to Zn 2p_{3/2} and Zn 2p_{1/2}, respectively (Fig. S15). All binding energies of Zn 2p_{3/2} in these catalysts appeared at almost the same position, between Zn (1021.1 eV) and ZnO (1022.0 eV), and closer to the ZnO at 1022.0 eV, indicating that the oxidation state of Zn in samples is close to + 2 [68]. According

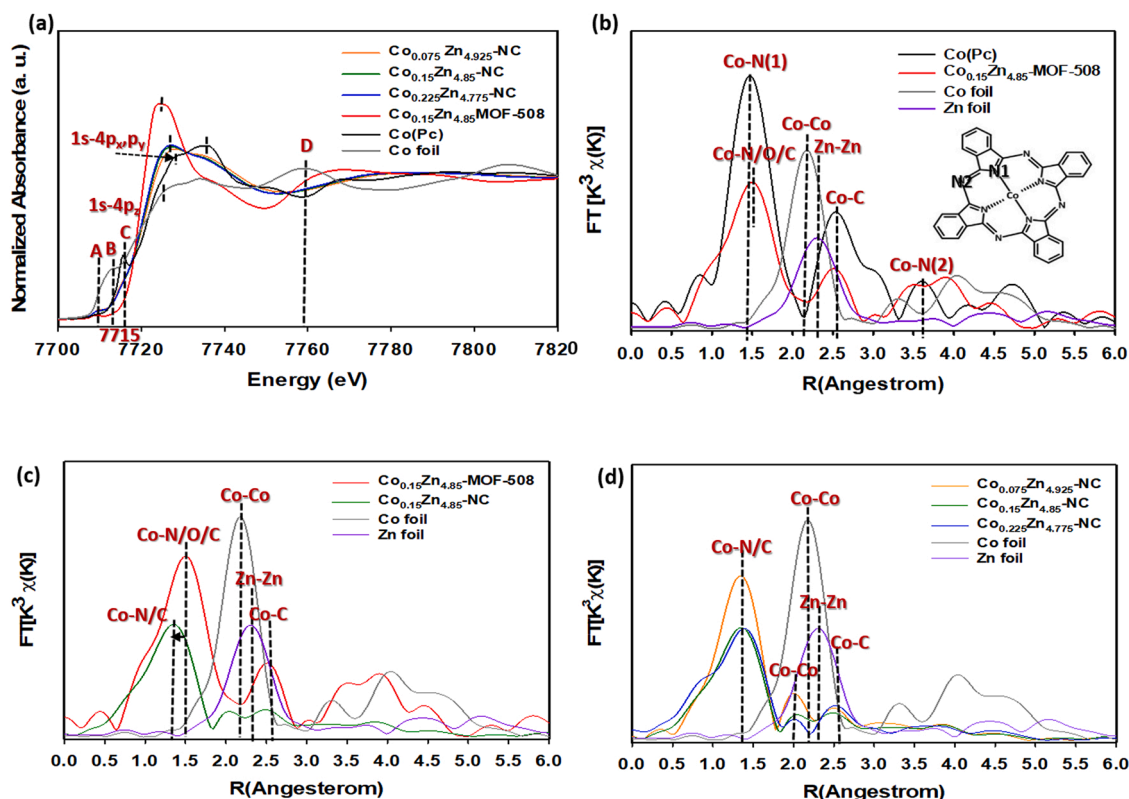


Fig. 3. (a) Co K-edge XANES spectra of the Co_xZn_y-NC and reference samples. (b-d) Fourier-transform EXAFS spectra of Co_xZn_y-NC and reference samples.

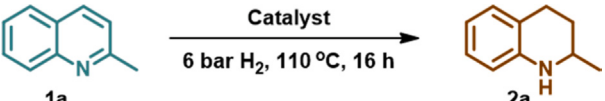
to previous reports, pyridinic N acts as a coordination site to form atomically dispersed M-N_x bonds in nitrogen-doped carbon materials [49].

Next, the oxidation state and local structures of the dispersed metal atoms in the pyrolyzed catalysts (Co_xZn_y-NC) were analyzed using X-ray absorption near-edge structure (XANES) and extended X-ray absorption fine structure measurements (EXAFS). Fig. 3a shows the XANES spectra at the Co K-edge of the Co_xZn_y-NC sample and standard samples of Co foil and cobalt phthalocyanine Co(Pc). A sharp pre-edge peak at 7715 eV (peak C) occurs due to the square-planar symmetry (D_{4h}) of the Co-N₄ structure of Co(Pc) [64,65]. The absence of a pre-edge peak at 7715 eV for Co_xZn_y-NC and Co/Zn-MOF-508 indicates different local symmetry of cobalt in the samples. A new pre-edge feature (peak A) appears at 7710 eV for Co_xZn_y-NC and Co/Zn-MOF-508. The decline in bonding energy of the pre-edge peak compared to Co(Pc) may show that cobalt in these structures experiences a lower oxidation state than that of Co(Pc). Moreover, peak A in Co/Zn-MOF-508 and pyrolyzed catalysts can be assigned to higher-coordinated cobalt sites in Co/Zn-MOF-508 or distorted local structures of atomically dispersed Co-N_x sites in pyrolyzed catalysts [69]. None of our samples (Co_xZn_y-NC and Co/Zn-MOF-508) depicted the spectral features of Co foil (peaks B, and D), indicating the dominant structure of cobalt in the prepared catalysts is atomic one. Furthermore, the Co K edge absorption threshold (white line peak position) for the pyrolyzed catalysts is located between cobalt foil and Co (Pc), indicating that the oxidation state of Co in the as-prepared catalysts is close to +2 [65].

Fourier transforms EXAFS spectrum of Co/Zn-MOF-508 show a similar main peak of cobalt phthalocyanine (Co-N1) at around 1.4 Å with a little positive shift due to the presence of four oxygen and one nitrogen coordination environment around the metal centers in the MOF frameworks (Fig. 3b). In addition, in the second coordination shell, there is the possibility of Co-C interaction at an R-value around 2.5 Å in the Co/Zn-MOF-508 (compared to Co(Pc)) EXAFS spectrum, the second coordination shell for Co-C appears at around 2.5 Å and the third one

belong to Co-N2 at around 3.5 Å (the Co(Pc) molecular structure, inset of Fig. 3b)) [64]. After pyrolysis, the intensity of the first coordinating shell decreased sharply and a blue shift can be observed in the R-value (near Co(Pc)), demonstrating changes in the coordination environment of Co metal by bonding with nitrogen atoms. Besides, a small peak around 2.1 Å appears near the Co-Co peak in the Co foil spectrum. A slight negative shift of the Co-Co peak in the pyrolyzed samples is related to the structural distortion of atomic Co sites during pyrolysis at high temperatures. Although, compared to the main peak (Co-N/C), the intensity of the second peak is much smaller, which confirms the atomic dispersion of Co metals distributed mainly as single Co-atoms in the structure of the catalyst (Fig. 3c). The EXAFS fitting results further reveal fine structural information of the pyrolyzed catalysts. Increasing the amount of Co precursor in the MOF resulted in a lower intensity Co-N/C peak, resulting in a reduced coordination number in the first coordinating shell (Fig. 3d). The average coordination number of catalyst Co_{0.075}Zn_{4.925}-NC is 4 and decreases to 3.8 and 3.7 for catalysts Co_{0.15}Zn_{4.85}-NC and Co_{0.225}Zn_{4.775}-NC, suggesting that Co-N_x consists of Co-N₃ and Co-N₄ in these two catalysts whilst it is mostly Co-N₄ in catalyst Co_{0.075}-NC (Table S3). The decreasing Co-N coordination number with increasing the Co content in the catalysts is also supported by decreasing surface N content as determined from XPS results (Table S4). The scissoring of some of the Co-N bonds in catalysts Co_{0.15}Zn_{4.85}-NC and Co_{0.225}Zn_{4.775}-NC raised the atomic defects around the single Co sites, which definitely influence the catalytic activity of the catalysts. In other words, the low Co content creates thermodynamically stable metal sites and synthesizes material with uniform atomically dispersed metal species on supports with few distinct adsorption sites. Non-uniform adsorption sites are formed with increasing the Co content due to the lack of availability of preferred sites on the support, and the potential of the species to be kinetically trapped in metastable sites leads to changes in the coordination number from 4 to 3.7, exhibiting the non-homogeneous local environment of cobalt sites on the support [70–72]. Similarly, Zn K-edge EXAFS spectra showed a main peak at

Table 1Optimization of the reaction conditions for the hydrogenation of quinaldine **1a**^a.

				
Entry	Catalyst	Solvent	Conv. (%) ^b	Sel. (%) ^b
1	Co _{0.15} Zn _{4.85} -NC	<i>i</i> -PrOH:H ₂ O	>99	>98, (94) ^c
2	Co _{0.15} Zn _{4.85} -NC	<i>n</i> -decane	27	>97
3	Co _{0.15} Zn _{4.85} -NC	mesitylene	31	>96
4	Co _{0.15} Zn _{4.85} -NC	<i>p</i> -xylene	40	>97
5	Co _{0.15} Zn _{4.85} -NC	toluene	52	99
6	Co _{0.15} Zn _{4.85} -NC	toluene:H ₂ O	56	>98
7	Co _{0.15} Zn _{4.85} -NC	<i>p</i> -xylene:H ₂ O	78 (98) ^d	99
8	Co _{0.15} Zn _{4.85} -NC	<i>i</i> -PrOH:H ₂ O	64 ^e	>97
9	Co _{0.15} Zn _{4.85} -NC	<i>i</i> -PrOH:H ₂ O	31 ^f	>97
10	NC	<i>i</i> -PrOH:H ₂ O	NR	-
11	Zn _{5.0} -NC	<i>i</i> -PrOH:H ₂ O	NR	-
12	Co _{0.075} Zn _{4.925} -NC	<i>i</i> -PrOH:H ₂ O	97	98
13	Co _{0.225} Zn _{4.775} -NC	<i>i</i> -PrOH:H ₂ O	98	>97
14	Co(Np)-NC	<i>i</i> -PrOH:H ₂ O	89	97

^a Conditions: 0.5 mmol of **1a**, 3.0 mol% of catalysts, 3 mL of solvents (2:1), 6 bar H₂ at 110 °C for 16 h.

^b Conversions were calculated from the corresponding peak area integrations of the reactant and product in the GC spectra. Selectivity was determined to correspond to 1,2,3,4-tetrahydroquinaldine (**2a**). NR = no reaction.

^c Number in the parentheses represents isolated yield after column chromatography.

^d For 24 h.

^e 2.0 mol% of Co_{0.15}Zn_{4.85}-NC.

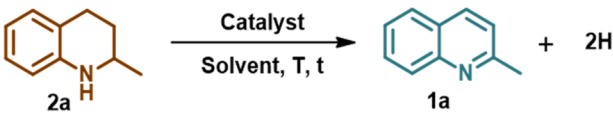
^f 1.0 mol% of Co_{0.15}Zn_{4.85}-NC.

1.5 Å, which could be attributed to Zn-N/C scattering paths of the first shell, and also has a small peak around 2.2 Å which is belonging to Zn-Zn bonding. The fitting results confirmed the coordination number of around 4 for Zn in the pyrolyzed catalysts. The EXAFS and XANES for Zn are reported in the [supplementary information](#) (Fig. S16).

3.2. Screening to find optimum condition for hydrogenation of quinaldine

We selected quinaldine **1a** as a model substrate to study the catalytic hydrogenation reaction under different conditions to find the optimum conditions for hydrogen storage. The results are summarized in [Table 1](#). At first, the effect of reaction H₂ pressure was screened using the catalyst Co_{0.15}Zn_{4.85}-NC (3 mol%) in 3 mL of *i*-PrOH:H₂O (2:1) as a solvent (see [Table S6](#)). Excellent results were achieved for converting quinaldine to 1,2,3,4-tetrahydroquinaldine at relatively low pressure using 6 bar H₂ at 110 °C for 16 h, and the product **2a** was isolated in 94% yield ([Table 1](#), entry 1). Next, several solvents such as *n*-decane, mesitylene, *p*-xylene, and toluene or mixed with water were examined to investigate the effect of solvent on this reaction. All of these proved to be inferior compared to *i*-PrOH:H₂O ([Table 1](#), entries 2–7). The conversion drastically decreased when the catalyst loading was reduced from 3 mol% to 1 mol%, and no formation of product **2a** was observed without a catalyst and NC catalyst ([Table 1](#), entries 8–10 and [Table S6](#)). Similarly, the conversion was decreased when reducing the reaction temperature or time ([Table S6](#)). Next, a zinc metal-anchored nitrogen-doped catalyst was tested to identify the catalytic activity of mixed metals of catalysts. Notably, a control experiment with Zn_{5.0}-NC catalyst failed to catalyze the hydrogenation reaction ([Table 1](#), entry 11). This result clearly indicates that cobalt metal is the leading active site for this catalytic hydrogenation reaction. After careful screening, the optimum reaction condition was found: 3 mol% of catalyst and 6 bar H₂ at 110 °C for 16 h. Next, different ratios of Co_xZn_y-NC catalysts were tested under optimized conditions for the hydrogenation process, and all of these showed high conversion ([Table 1](#), entries 12–13). Moreover, the Co(Np)-NC catalyst showed lower activity under the standard reaction conditions ([Table 1](#),

Table 2Optimization of the reaction conditions for the dehydrogenation of 1,2,3,4-tetrahydroquinaldine **2a**^a.

						
Entry	Catalyst	Solvent	T (°C)	t (h)	Conv. (%) ^b	Sel. (%) ^b
1	Co _{0.15} Zn _{4.85} -NC	<i>p</i> -xylene:H ₂ O	200	24	79, >99 ^c	>98
2	Co _{0.15} Zn _{4.85} -NC	<i>i</i> -PrOH:H ₂ O	200	24	>99	>98
3	Co _{0.15} Zn _{4.85} -NC	<i>i</i> -PrOH:H ₂ O	180	24	66	>98
4	Co _{0.15} Zn _{4.85} -NC	<i>i</i> -PrOH:H ₂ O	160	24	41	>98
5	Co _{0.15} Zn _{4.85} -NC	<i>i</i> -PrOH:H ₂ O	200	20	>99	>98, (93) ^d
6	Co _{0.15} Zn _{4.85} -NC	<i>i</i> -PrOH:H ₂ O	200	12	85	99
7	Co _{0.15} Zn _{4.85} -NC	<i>i</i> -PrOH:H ₂ O	200	20	87 ^e	99
8	Co _{0.15} Zn _{4.85} -NC	<i>i</i> -PrOH:H ₂ O	200	20	56 ^f	>98
9	No catalyst	<i>i</i> -PrOH:H ₂ O	200	20	trace	-
10	NC	<i>i</i> -PrOH:H ₂ O	200	20	20	90
11	Zn _{5.0} -NC	<i>i</i> -PrOH:H ₂ O	200	20	12	>87
12	Co _{0.075} Zn _{4.925} -NC	<i>i</i> -PrOH:H ₂ O	200	20	90	>98
13	Co _{0.225} Zn _{4.775} -NC	<i>i</i> -PrOH:H ₂ O	200	20	85	>98
14	Co(Np)-NC	<i>i</i> -PrOH:H ₂ O	200	20	88	>94

^a Conditions: 0.5 mmol of **2a**, 3.0 mol% of catalysts, 3 mL of solvents (2:1), 12–24 h at 160–200 °C.

^b Conversions were calculated from the relative peak area integrations of the reactant and product in the GC spectra. Selectivity was determined corresponding to quinaldine (**1a**).

^c For 30 h.

^d Number in the parentheses represent isolated yield after column chromatography.

^e 2.0 mol% Co_{0.15}Zn_{4.85}-NC.

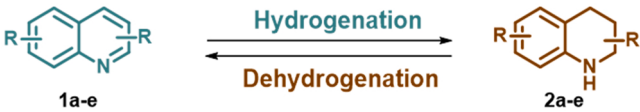
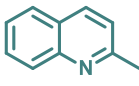
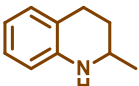
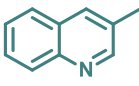
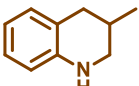
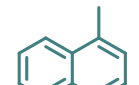
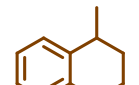
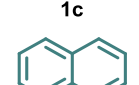
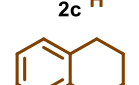
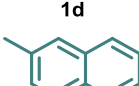
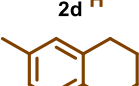
^f 1.0 mol% Co_{0.15}Zn_{4.85}-NC. NR = no reaction.

entry 14). These results highlight that atomically dispersed Co_xZn_y-NC was an excellent catalyst for the hydrogen storage reaction, suggesting that the hierarchically porous structure of the catalyst could expose more active sites and be beneficial to the transfer of reactant and product species, resulting in higher catalytic activity.

3.3. Screening to find optimum condition for dehydrogenation of 1,2,3,4-tetrahydroquinaldine

Next, we turned our attention to the acceptor-less dehydrogenation of 1,2,3,4-tetrahydroquinaldine **2a** to release hydrogen gas and investigated the catalysts for suitability in a reversible dehydrogenation/hydrogenation system. Initially, we performed the reaction with 0.5 mmol of **2a**, 3 mol% of Co_{0.15}Zn_{4.85}-NC at 160 °C for 24 h in 3 mL of *p*-xylene:H₂O (2:1) as a solvent and the desired product **1a** was obtained in only 17% conversion (see [Table S7](#)). By increasing the reaction temperature to 200 °C for 24 h, we saw a significantly improved conversion of **2a** to 79%, and quantitative conversion (>99%) was achieved for **2a** after a longer reaction time 30 h ([Table 2](#), entry 1). Interestingly, when *i*-PrOH:H₂O (2:1) was used as the solvent, the dehydrogenation reaction completely converted **2a** to **1a** within 24 h at 200 °C ([Table 2](#), entry 2). Therefore, *i*-PrOH:H₂O solvent was selected for further screening due to

Table 3Co_{0.15}Zn_{4.85}-NC catalyzed hydrogenation and dehydrogenation of various quinoline derivatives..

<div style="text-align: center;">  </div>						
S.No	Substrate (1a-e) ^a	Substrate (2a-e) ^b	Hydrogenation		Dehydrogenation	
			Conv. (%) ^c	Yield (%) ^d	Conv. (%) ^c	Yield (%) ^d
1			100	94	100	93
2			80	75	56	50
3			NA	18	NA	55
4			68	62	80	73
5			76	72	94	89

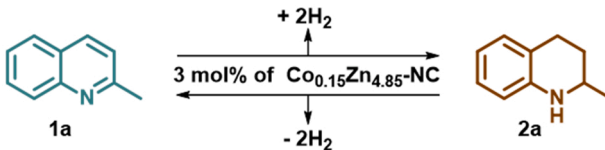
^a Hydrogenation: 0.5 mmol of **1a–e**, 3.0 mol% of Co_{0.15}Zn_{4.85}-NC, 3 mL of *i*-PrOH:H₂O (2:1), 6 bar H₂ at 110 °C for 16 h.^b Dehydrogenation: 0.5 mmol of **2a–e**, 3.0 mol% of Co_{0.15}Zn_{4.85}-NC, 3 mL of *i*-PrOH:H₂O (2:1) at 200 °C, 20 h.^c Conversions were calculated from the relative peak area integrations of the reactant and product in the GC spectra. NA = not available, GC signal for **1c** and **2c** is not separated.^d Yield of isolated product after column chromatography.

its high catalytic activity. When the temperature decreased from 200 °C to 160 °C, the conversions decreased sharply from >99–41% (Table 2, entries 3–4), and therefore, a temperature of 200 °C was critical for this reaction. To our delight, the complete conversion of **2a** into quinaldine **1a** was observed after 20 h, and product **1a** was isolated in 93% yield (Table 2, entry 5). The identity of the gas formed in this reaction was qualitatively analyzed by gas chromatography, which unequivocally confirmed the formation of pure H₂ gas from the dehydrogenation reaction (Fig. S17). An attempt to decrease the reaction time further led to an incomplete transformation of **2a** (Table 2, entry 6). On the other hand, reducing the catalyst to 1 mol% resulted in a lower conversion of **2a** at 200 °C in 20 h (Table 2, entries 7–8). We concluded that the best result of complete conversion of **2a** was obtained using 3 mol% of catalyst in *i*-PrOH:H₂O (2:1) at 200 °C for 20 h. In the absence of a catalyst, only a trace amount of dehydrogenation product formed under typical reaction conditions (Table 2, entry 9). A control experiment with a NC and Zn_{5.0}-NC catalyst showed a very low conversion of **2a** (Table 2, entries 10–11). We believed this low activity was due to heteroatom-doped carbon in the support [34] and clearly indicated that Co was the primary metal active site for the dehydrogenation reaction. Other catalysts, such as Co_{0.075}Zn_{4.925}-NC, Co_{0.225}Zn_{4.775}-NC and Co(Np)-NC, were tested for their catalytic activity under established conditions (Table 2, entries 12–14). To our delight, Co_{0.15}Zn_{4.85}-NC showed the highest catalytic activity for the dehydrogenation of 1,2,3,4-tetrahydroquinoline to quinaldine. Furthermore, ICP-OES analysis of the filtrate suggested no significant catalyst leaching during the reaction. The results demonstrate that the use of 3.0 mol% of Co_{0.15}Zn_{4.85}-NC is an efficient catalyst for the reversible dehydrogenation and hydrogenation

of quinoline derivatives, comparable to previously reported non-precious metal heterogeneous catalysts required high-loading of catalyst [Tables S8–S10] [32–34].

Furthermore, the emerging atomically dispersed metal catalysts, with definite structures as active sites provide the possibility to explore the structure-activity relationship.[69,73,74] The difference in the catalytic activity of Co_xZn_y-NC catalysts is explained by the local coordination environment of the cobalt active sites embedded in porous and conductive support is greatly desired [71]. For the hydrogenation reaction, all three single atomic catalysts with different cobalt contents exhibit almost similar reactivity and selectivity. The EXAFS fitting results reveal that the structure of Co_{0.075}Zn_{4.925}-NC is Co-N₄ active site, and the Co_{0.15}Zn_{4.85}-NC and Co_{0.225}Zn_{4.775}-NC catalysts contain a mixture of Co-N₃ and Co-N₄ as active sites. The obtained results indicate that both Co-N₃ and Co-N₄ are active sites for this hydrogenation reaction. For the dehydrogenation reaction, 90% conversion was obtained with Co_{0.075}Zn_{4.925}-NC, and when the Co content in Co_{0.15}Zn_{4.85}-NC raised to 0.15, the reactivity increased to >99% conversion with the same selectivity; but the reactivity decreased to 85% conversion with further increasing of the Co content to 0.225 in Co_{0.225}Zn_{4.775}-NC. Based on the differences in the local coordination environment in these three catalysts, we can propose in the first enhancement of the cobalt amount we will have a mixture of Co-N₄ and Co-N₃ sites which show different reactivity to dehydrogenation reaction but based on the reactivity improvement we can suggest that in this step the amount of more active coordination environment has increased on the support. But in the second step of increasing cobalt content, although, we obtained the same coordination number and we had a mixture of Co-N₄ and Co-N₃

Table 4Reversible hydrogenation/dehydrogenation of 1a/2a catalyzed by Co_{0.15}Zn_{4.85}-NC.

				
Cycle ^a	Hydrogenation ^b		Dehydrogenation ^c	
	Conv. (%) ^d	Sel. (%) ^d	Conv. (%) ^d	Sel. (%) ^d
1	>99	>98	>99	>98
2	98	>98	99	98
3	98	98	98	>97

^a Cycle: A complete run of one hydrogenation and one dehydrogenation reactions.^b Hydrogenation: 0.5 mmol of **1a**, 3.0 mol% of Co_{0.15}Zn_{4.85}-NC, 3 mL of *i*-PrOH:H₂O (2:1), 6 bar H₂ at 110 °C for 16 h.^c Dehydrogenation: 200 °C, 20 h.^d Conversions were calculated from the relative peak area integrations of the reactant and product in the GC spectra. Selectivity was determined corresponding to product.

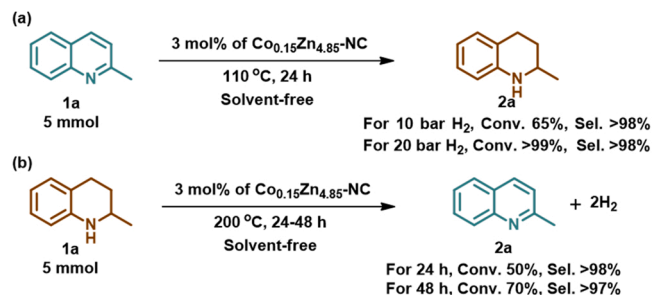
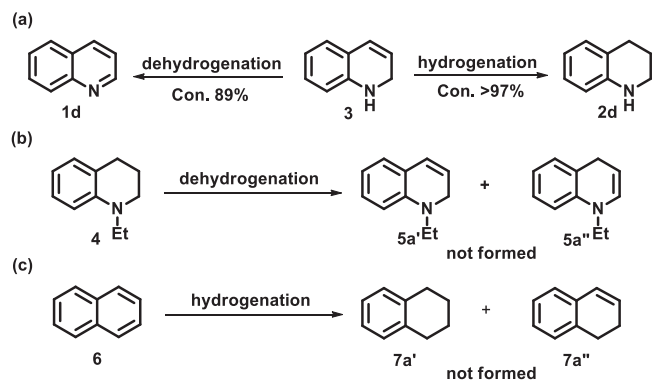
sites for cobalt but the ratio of the less active environment is higher than the more active one and because of that we saw a clear decrease in reactivity. In summary, with this much study on the local environment of cobalt sites, we cannot say surely which of the Co-N₃ or Co-N₄ sites are more active in dehydrogenation reaction; detailed DFT calculation needs to study the reactivity toward dehydrogenation and define the mechanism that will be studied in our next manuscript.

3.4. Scope of hydrogenation and dehydrogenation of quinoline derivatives

To identify efficient hydrogen storage systems, we next investigated the scope of this reversible hydrogenation and dehydrogenation reaction with a series of quinoline derivatives under optimized reaction conditions. The results are shown in Table 3. The hydrogenation of 3- and 6-methylquinolines (**1b** & **1e**) under the optimized conditions led to 80% and 76% conversion (**2b** & **2e**), respectively, whereas the 4-methylquinoline **1c** gave inferior conversion. Similarly, quinoline **1e** undergoes a moderate reaction under the same conditions, achieving only 68% conversion. Next, the dehydrogenation of substituted 1,2,3,4-tetrahydroquinoline derivatives (**2b–d**) under standard reaction conditions afforded the dehydrogenated product (**1b–d**) in moderate to good conversions. Notably, substrate **2e** underwent smooth dehydrogenation and furnished the desired product **1e** at 94% conversion.

3.5. Reversible and repetitive transformations between 1a and 2a

Based on the complete conversion of compounds **1a** and **2a**, we selected them as a hydrogen storage system to study the reversible and repetitive transformations between **1a** and **2a** via hydrogenation and dehydrogenation reactions using Co_{0.15}Zn_{4.85}-NC as a single catalyst and the results are shown in Table 4. First, the hydrogenation of **1a** was carried out in a steel autoclave reactor using 3.0 mol% of Co_{0.15}Zn_{4.85}-NC, 3 mL of *i*-PrOH:H₂O (2:1), 6 bar H₂ at 110 °C for 16 h, resulting in the complete conversion of **1a** into **2a**. Next, the same reaction mixture was continued for dehydrogenation at 200 °C for 20 h in the same autoclave, and full conversion was obtained. Notably, this reversible hydrogen store/release was demonstrated for three consecutive cycles without loss of catalytic activity. These experiments highlight that the catalyst is stable and conveniently reused without being deactivated during the reaction. Furthermore, the catalyst was recovered and characterized by HR-TEM and XPS. As shown in Fig. S18, no obvious nanoparticles were observed in the TEM images of the recycled catalyst,

**Scheme 2.** Reversible hydrogenation/dehydrogenation of **1a/2a** under solvent-free conditions.**Scheme 3.** Control experiments.

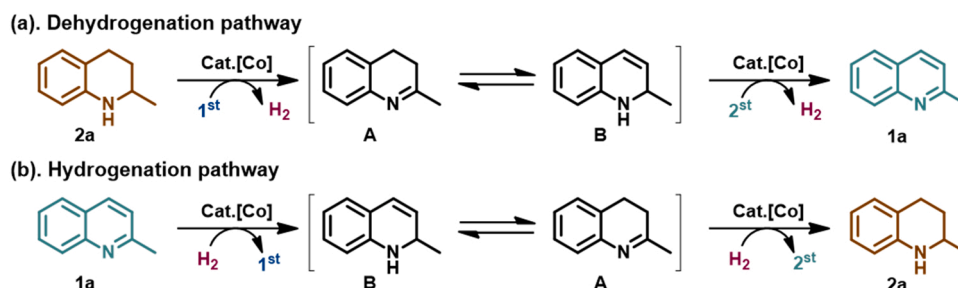
which was consistent with the ring-like SAED pattern, resulting in no crystalline nanoparticles. These results demonstrated that the metal atoms were still uniformly distributed in the structure even after six runs, confirming the robustness of the catalyst during the reactions. The high-resolution XPS spectra of the recycled catalyst in the Co 2p region were further investigated, indicating that there was no significant change in the position of the peaks in the fresh and recycled catalyst (Fig. S19).

3.6. Solvent-free condition for hydrogenation/dehydrogenation of 1a/2a

Furthermore, we attempted reversible hydrogenation/dehydrogenation of **1a** and **2a** under solvent-free conditions to develop an environmentally friendly hydrogen storage system (Scheme 2). Generally, a solvent-free hydrogenation reaction requires high pressure and a long reaction time. Initially, the reaction was carried out with 5 mmol of **1a**, 3.0 mol% of Co_{0.15}Zn_{4.85}-NC and 10 bar H₂ at 110 °C for 24 h, obtaining 65% conversion, and a complete conversion (>99%) was accomplished at 20 bar H₂ (Scheme 2a). However, the dehydrogenation reaction reached good conversion (70%) even with a longer reaction time compared with the case using a solvent (Scheme 2b). To the best of our knowledge, the solvent-free condition was studied for both hydrogenation and dehydrogenation of quinoline derivatives for the first time using a single heterogeneous catalyst.

3.7. Control experiments and possible reaction mechanism

A series of control experiments were performed to understand the reaction mechanism for dehydrogenation/hydrogenation of quinolines under standard conditions (Scheme 3). First, we carried out the dehydrogenation and hydrogenation reaction with 1,2-dihydroquinoline **3**, which undergoes a reaction under standard reaction conditions, leading to products **1d** and **2d**, respectively. When 1-ethyl-1,2,3,4-tetrahydroquinoline **4** was subjected to the standard catalytic conditions, the



Scheme 4. Proposed mechanism of the dehydrogenation and hydrogenation reactions.

dehydrogenated product **5** was not formed. These results clearly suggest that the free N-H bond is vital for a successful reaction and presumably supports the isomerization step. Furthermore, the hydrogenation reaction of naphthalene **6** failed to proceed under the present conditions, indicating that nitrogen is indispensable for the reaction.

Based on the control experiment results and existing reports [31,33], we proposed a possible mechanism for the dehydrogenation and hydrogenation reaction in Scheme 4. Initially, **2a** binds to the cobalt surface of the catalyst via nitrogen, activating N-H and adjacent C-H bonds and liberating the first equivalent of H_2 through a dehydrogenation reaction to give the intermediate **A**. Before releasing the second equivalent of H_2 , intermediate **A** isomerizes to form **B**, followed by subsequent dehydrogenation involving the same N-H and adjacent C-H bonds to give the fully dehydrogenated product **1a**. For hydrogenation, **1a** similarly binds to the cobalt surface of the catalyst via nitrogen, followed by the first hydrogenation of the activated ring near the C=N double bond to form partially hydrogenated intermediate **B**. Next, second hydrogenation occurs via two different pathways, either direct alkene hydrogenation at the remaining C=C double bond of **B** or with isomerized intermediate C=N double bond of **A**, to give the final product **2a**.

4. Conclusion

In summary, we have successfully prepared atomically dispersed Co/Zn single-atoms on a nitrogen-doped carbon material as an efficient single heterogeneous catalyst for the reversible hydrogenation and acceptor-less dehydrogenation of quinolines to store and release H_2 in the same solvent. Notably, 3 mol% of $Co_{0.15}Zn_{4.85}$ -NC catalysts showed outstanding catalytic activity for both reactions compared to the reported heterogeneous non-precious metal catalysts that required higher loading of catalysts. This catalyst demonstrated three consecutive cycles of hydrogen storage/release through reversible hydrogenation/dehydrogenation processes under optimized conditions. Moreover, the catalyst is highly efficient, robust, and reusable many times without loss of catalytic efficiency. To the best of our knowledge, both hydrogenation and dehydrogenation of quinoline derivatives were studied under solvent-free conditions for the first time. A possible reaction mechanism was proposed based on control experiment results and previous reports, which revealed that the free N-H group/N-atom is crucial for the success of reversible dehydrogenation/hydrogenation reaction. This work will stimulate researchers to use new MOFs to prepare MOF-derived metal single-atom catalysts for various catalytic applications. Further studies are underway to develop more efficient single heterogeneous catalysts for the reversible dehydrogenation/hydrogenation of homocyclic compounds with high hydrogen content.

CRediT authorship contribution statement

Kanagaraj Naveen: Conceptualization, Methodology, Data curation, Validation, Formal analysis, Investigation, Writing – original draft, Writing – review & editing, Experiment design. **Tahereh Mahvelati-Shamsabadi:** Writing – review & editing. **Pragyan Sharma:**

Experimental work for revision. **Seong-hun Lee:** EXFAS studies and discussion. **Seung Hyun Hur:** Supervision. **Won Mook Choi:** Supervision. **Tae Joo Shin:** EXFAS studies and discussion. **Jin Suk Chung:** Project administration, Funding acquisition, Supervision, Writing – review & editing.

Declaration of Competing Interest

The authors declare that they have no known competing financial interests or personal relationships that could have appeared to influence the work reported in this paper.

Data availability

Data will be made available on request.

Acknowledgements

This study was supported by the National Research Foundation of Korea (NRF) grant funded by the Korea government (MSIT) (2020R1A4A4079954) and Priority Research Centers Program (MOE) (2021R1A6A1A03038858). This result was also supported by the Regional Innovation Strategy (RIS) through the National Research Foundation of Korea (NRF) funded by the Ministry of Education (MOE) (2021RIS-003).

Experiments at PLS-II 6D UNIST-PAL beamline were supported in part by MSIT, POSTECH, and UNIST Central Research Facilities.

Appendix A. Supporting information

Supplementary data associated with this article can be found in the online version at [doi:10.1016/j.apcatb.2023.122482](https://doi.org/10.1016/j.apcatb.2023.122482).

References

- [1] K. Mazloomi, C. Gomes, Hydrogen as an energy carrier: prospects and challenges, *Renew. Sustain. Energy Rev.* 16 (2012) 3024–3033.
- [2] K.T. Møller, T.R. Jensen, E. Akiba, H. Li, Hydrogen - a sustainable energy carrier, *Prog. Nat. Sci. Mater. Int.* 27 (2017) 34–40.
- [3] J.O. Abe, A.P.I. Popoola, E. Ajenifuja, O.M. Popoola, Hydrogen energy, economy and storage: review and recommendation, *Int. J. Hydrog. Energy* 44 (2019) 15072–15086.
- [4] A.F. Dalebrook, W. Gan, M. Grasemann, S. Moret, G. Laurenczy, Hydrogen storage: beyond conventional methods, *Chem. Commun.* 49 (2013) 8735–8751.
- [5] J. Andersson, S. Grönkvist, Large-scale storage of hydrogen, *Int. J. Hydrog. Energy* 44 (2019) 11901–11919.
- [6] M.R. Usman, Hydrogen storage methods: review and current status, *Renew. Sustain. Energy Rev.* 167 (2022), 112743.
- [7] P.T. Aakko-Saksa, C. Cook, J. Kiviahio, T. Repo, Liquid organic hydrogen carriers for transportation and storing of renewable energy - review and discussion, *J. Power Sources* 396 (2018) 803–823.
- [8] Z. Abidin, C. Tang, Y. Liu, K. Catchpole, Large-scale stationary hydrogen storage via liquid organic hydrogen carriers, *iScience* 24 (2021), 102966.
- [9] P.M. Modisha, C.N.M. Ouma, R. Garidzirai, P. Wasserscheid, D. Bessarabov, The prospect of hydrogen storage using liquid organic hydrogen carriers, *Energy Fuels* 33 (2019) 2778–2796.
- [10] Q.-L. Zhu, Q. Xu, Liquid organic and inorganic chemical hydrides for high-capacity hydrogen storage, *Energy Environ. Sci.* 8 (2015) 478–512.

- [11] P.C. Rao, M. Yoon, Potential liquid-organic hydrogen carrier (LOHC) systems: a review on recent progress, *Energies* 13 (2020) 6040.
- [12] R.H. Crabtree, Hydrogen storage in liquid organic heterocycles, *Energy Environ. Sci.* 1 (2008) 134–138.
- [13] J. Oh, K. Jeong, T.W. Kim, H. Kwon, J.W. Han, J.H. Park, Y.-W. Suh, 2-(N-Methylbenzyl)pyridine: a potential liquid organic hydrogen carrier with fast H₂ release and stable activity in consecutive cycles, *ChemSusChem* 11 (2018) 661–665.
- [14] Y. Xie, D. Milstein, Pd catalyzed, acid accelerated, rechargeable, liquid organic hydrogen carrier system based on methylpyridines/methylpiperidines, *ACS Appl. Energy Mater.* 2 (2019) 4302–4308.
- [15] M.S. Salman, N. Rambhujun, C. Prathana, K. Srivastava, K.-F. Aguey-Zinsou, Catalysis in liquid organic hydrogen storage: recent advances, challenges, and perspectives, *Ind. Eng. Chem. Res.* 61 (2022) 6067–6105.
- [16] T.W. Kim, H. Jeong, J.H. Baik, Y.-W. Suh, State-of-the-art catalysts for hydrogen storage in liquid organic hydrogen carriers, *Chem. Lett.* 51 (2022) 239–255.
- [17] J. Wu, J.H. Barnard, Y. Zhang, D. Talwar, C.M. Robertson, J. Xiao, Robust cyclometallated Ir(III) catalysts for the homogeneous hydrogenation of N-heterocycles under mild conditions, *Chem. Commun.* 49 (2013) 7052–7054.
- [18] F. Chen, A.-E. Surkus, L. He, M.-M. Pohl, J. Radnik, C. Topf, K. Junge, M. Beller, Selective catalytic hydrogenation of heteroarenes with N-graphene-modified cobalt nanoparticles (Co₃O₄-Co/NGr@ α -Al₂O₃), *J. Am. Chem. Soc.* 137 (2015) 11718–11724.
- [19] Z. Wei, Y. Chen, J. Wang, D. Su, M. Tang, S. Mao, Y. Wang, Cobalt encapsulated in N-doped graphene layers: an efficient and stable catalyst for hydrogenation of quinoline compounds, *ACS Catal.* 6 (2016) 5816–5822.
- [20] Q. Wang, H. Chai, Z. Yu, Acceptorless dehydrogenation of N-heterocycles and secondary alcohols by Ru(II)-NNC complexes bearing a pyrazolyl-indolylpyridine ligand, *Organometallics* 37 (2018) 584–591.
- [21] J. Wu, D. Talwar, S. Johnston, M. Yan, J. Xiao, Acceptorless dehydrogenation of nitrogen heterocycles with a versatile iridium catalyst, *Angew. Chem. Int. Ed.* 52 (2013) 6983–6987.
- [22] S.K. Moromi, S.M.A.H. Siddiki, K. Kon, T. Toyao, K. Shimizu, Acceptorless dehydrogenation of N-heterocycles by supported Pt catalysts, *Catal. Today* 281 (2017) 507–511.
- [23] S. Chakraborty, W.W. Brennessel, W.D. Jones, A molecular iron catalyst for the acceptorless dehydrogenation and hydrogenation of N-heterocycles, *J. Am. Chem. Soc.* 136 (2014) 8564–8567.
- [24] R. Xu, S. Chakraborty, H. Yuan, W.D. Jones, Acceptorless, reversible dehydrogenation and hydrogenation of N-heterocycles with a cobalt pincer catalyst, *ACS Catal.* 5 (2015) 6350–6354.
- [25] Y. Han, Z. Wang, R. Xu, W. Zhang, W. Chen, L. Zheng, J. Zhang, J. Luo, K. Wu, Y. Zhu, C. Chen, Q. Peng, Q. Liu, P. Hu, D. Wang, Y. Li, Ordered porous nitrogen-doped carbon matrix with atomically dispersed cobalt sites as an efficient catalyst for dehydrogenation and transfer hydrogenation of n-heterocycles, *Angew. Chem. Int. Ed.* 57 (2018) 11262–11266.
- [26] G. Jaiswal, M. Subramanian, M.K. Sahoo, E. Balaraman, A reusable cobalt catalyst for reversible acceptorless dehydrogenation and hydrogenation of N-heterocycles, *ChemCatChem* 11 (2019) 2449–2457.
- [27] R. Yamaguchi, C. Ikeda, Y. Takahashi, K. Fujita, Homogeneous catalytic system for reversible dehydrogenation-hydrogenation reactions of nitrogen heterocycles with reversible interconversion of catalytic species, *J. Am. Chem. Soc.* 131 (2009) 8410–8412.
- [28] A. Vivanco, M. Beller, M. Albrecht, NHC-based iridium catalysts for hydrogenation and dehydrogenation of N-heteroarenes in water under mild conditions, *ACS Catal.* 8 (2018) 17–21.
- [29] C. Deraedt, R. Ye, W.T. Ralston, F.D. Toste, G.A. Somorjai, Dendrimer-stabilized metal nanoparticles as efficient catalysts for reversible dehydrogenation/hydrogenation of N-heterocycles, *J. Am. Chem. Soc.* 139 (2017) 18084–18092.
- [30] J.-W. Zhang, D.-D. Li, G.-P. Lu, T. Deng, C. Cai, Reversible dehydrogenation and hydrogenation of N-heterocycles catalyzed by bimetallic nanoparticles encapsulated in MIL-100(Fe), *ChemCatChem* 10 (2018) 4966–4972.
- [31] X. Cui, Z. Huang, A.P. van Muyden, Z. Fei, T. Wang, P.J. Dyson, Acceptorless dehydrogenation and hydrogenation of N- and O-containing compounds on Pd₃Au₁(111) facets, *Sci. Adv.* 6 (2020), eabb3831.
- [32] Y. Mikami, K. Ebata, T. Mitsudome, T. Mizugaki, K. Jitsukawa, K. Kaneda, Reversible dehydrogenation-hydrogenation of tetrahydroquinoline-quinoline using a supported copper nanoparticle catalyst, *Heterocycles* 82 (2010) 1371–1377.
- [33] P. Ryabchuk, A. Agapova, C. Kreyenschulte, H. Lund, H. Junge, K. Junge, M. Beller, Heterogeneous nickel-catalysed reversible, acceptorless dehydrogenation of N-heterocycles for hydrogen storage, *Chem. Commun.* 55 (2019) 4969–4972.
- [34] H. Su, L.-H. Sun, Z.-H. Xue, P. Gao, S.-N. Zhang, G.-Y. Zhai, Y.-M. Zhang, Y.-X. Lin, X.-H. Li, J.-S. Chen, Nitrogen-thermal modification of the bifunctional interfaces of transition metal/carbon dyads for the reversible hydrogenation and dehydrogenation of heteroarenes, *Chem. Commun.* 55 (2019) 11394–11397.
- [35] Y. Chen, S. Ji, C. Chen, Q. Peng, D. Wang, Y. Li, Single-atom catalysts: synthetic strategies and electrochemical applications, *Joule* 2 (2018) 1242–1264.
- [36] T. Sun, L. Xu, D. Wang, Y. Li, Metal organic frameworks derived single atom catalysts for electrocatalytic energy conversion, *Nano Res.* 12 (2019) 2067–2080.
- [37] H. Yan, C. Su, J. He, W. Chen, Single-atom catalysts and their applications in organic chemistry, *J. Mater. Chem. A* 6 (2018) 8793–8814.
- [38] L. Sun, L. Han, J. Huang, X. Luo, X. Li, Single-atom catalysts for photocatalytic hydrogen evolution: a review, *Int. J. Hydrog. Energy* 47 (2022) 17583–17599.
- [39] Z. Song, L. Zhang, K. Doyle-Davis, X. Fu, J.-L. Luo, X. Sun, Recent advances in MOF-derived single atom catalysts for electrochemical applications, *Adv. Energy Mater.* 10 (2020), 2001561.
- [40] Z. Pu, I.S. Amiin, R. Cheng, P. Wang, C. Zhang, S. Mu, W. Zhao, F. Su, G. Zhang, S. Liao, S. Sun, Single-atom catalysts for electrochemical hydrogen evolution reaction: recent advances and future perspectives, *Nano Micro Lett.* 12 (2020) 21.
- [41] L. Zou, Y.-S. Wei, C.-C. Hou, C. Li, Q. Xu, Single-atom catalysts derived from metal-organic frameworks for electrochemical applications, *Small* 17 (2021), 2004809.
- [42] H. Huang, K. Shen, F. Chen, Y. Li, Metal-organic frameworks as a good platform for the fabrication of single-atom catalysts, *ACS Catal.* 10 (2020) 6579–6586.
- [43] Y. Ye, F. Cai, H. Li, H. Wu, G. Wang, Y. Li, S. Miao, S. Xie, R. Si, J. Wang, X. Bao, Surface functionalization of ZIF-8 with ammonium ferric citrate toward high exposure of Fe-N active sites for efficient oxygen and carbon dioxide electroreduction, *Nano Energy* 38 (2017) 281–289.
- [44] Z. Qin, H. Li, X. Yang, L. Chen, Y. Li, K. Shen, Heterogenizing homogeneous cocatalysts by well-designed hollow MOF-based nanoreactors for efficient and size-selective CO₂ fixation, *Appl. Catal. B Environ.* 307 (2022), 121163.
- [45] H. Li, Z. Qin, X. Yang, X. Chen, Y. Li, K. Shen, Growth pattern control and nanoarchitecture engineering of metal-organic framework single crystals by confined space synthesis, *ACS Cent. Sci.* 8 (2022) 718–728.
- [46] Y. Wu, L. Chen, X. Yang, Y. Li, K. Shen, Facet-selective growth of MOF-on-MOF heterostructures enables etching-free synthesis of highly-open Co/N-doped carbon nanoframes for efficient catalysis, *Sci. China Chem.* 65 (2022) 2450–2461.
- [47] V. Pascanu, G.G. Miera, A.K. Inge, B. Martín-Matute, Metal-organic frameworks as catalysts for organic synthesis: a critical perspective, *J. Am. Chem. Soc.* 141 (2019) 7223–7234.
- [48] A. Bavykina, N. Kolobov, I.S. Khan, J.A. Bau, Galilea, A. Ramirez, J. Gascon, Metal-organic frameworks in heterogeneous catalysis: recent progress, new trends, and future perspectives, *Chem. Rev.* 120 (2020) 8468–8535.
- [49] A. Han, B. Wang, A. Kumar, Y. Qin, J. Jin, X. Wang, C. Yang, B. Dong, Y. Jia, J. Liu, X. Sun, Recent advances for MOF-derived carbon-supported single-atom catalysts, *Small Methods* (2019), 1800471.
- [50] J. Hwang, A review of synthesis strategies for MOF-derived single atom catalysts, *Korean J. Chem. Eng.* 38 (2021) 1104–1116.
- [51] X. Wang, W. Chen, L. Zhang, T. Yao, W. Liu, Y. Lin, H. Ju, J. Dong, L. Zheng, W. Yan, X. Zheng, Z. Li, X. Wang, J. Yang, D. He, Y. Wang, Z. Deng, Y. Wu, Y. Li, Uncoordinated amine groups of metal-organic frameworks to anchor single Ru sites as chemoselective catalysts toward the hydrogenation of quinoline, *J. Am. Chem. Soc.* 139 (2017) 9419–9422.
- [52] Y. Yang, K. Mao, S. Gao, H. Huang, G. Xia, Z. Lin, P. Jiang, C. Wang, H. Wang, Q. Chen, O-, N-atoms-coordinated Mn cofactors within a graphene framework as bioinspired oxygen reduction reaction electrocatalysts, *Adv. Mater.* 30 (2018), 1801732.
- [53] E. Zhang, T. Wang, K. Yu, J. Liu, W. Chen, A. Li, H. Rong, R. Lin, S. Ji, X. Zheng, Y. Wang, L. Zheng, C. Chen, D. Wang, J. Zhang, Y. Li, Bismuth single atoms resulting from transformation of metal-organic frameworks and their use as electrocatalysts for CO₂ reduction, *J. Am. Chem. Soc.* 141 (2019) 16569–16573.
- [54] Y.N. Gong, L. Jiao, Y. Qian, C.Y. Pan, L. Zheng, X. Cai, B. Liu, S.-H. Yu, H.-L. Jiang, Regulating the coordination environment of MOF-templated single-atom nickel electrocatalysts for boosting CO₂ reduction, *Angew. Chem. Int. Ed.* 59 (2020) 2705–2709.
- [55] W.-H. Li, B.-C. Ye, J. Yang, Y. Wang, C.-J. Yang, Y.-M. Pan, H.-T. Tang, D. Wang, Y. Li, A single-atom cobalt catalyst for the fluorination of acyl chlorides at parts-per-million catalyst loading, *Angew. Chem. Int. Ed.* 61 (2022), e202209749.
- [56] Y. Xiong, W. Sun, Y. Han, P. Xin, X. Zheng, W. Yan, J. Dong, J. Zhang, D. Wang, Y. Li, Cobalt single atom site catalysts with ultrahigh metal loading for enhanced aerobic oxidation of ethylbenzene, *Nano Res.* 14 (2021) 2418–2423.
- [57] X. Li, A.-E. Surkus, J. Rabeah, M. Anwar, S. Dastgir, H. Junge, A. Brückner, M. Beller, Cobalt single-atom catalysts with high stability for selective dehydrogenation of formic acid, *Angew. Chem. Int. Ed.* 59 (2020) 15849–15854.
- [58] X. Sun, A.I. Olivos-Suarez, D. Osadchii, M.J.V. Romero, F. Kapteijn, J. Gascon, Single cobalt sites in mesoporous N-doped carbon matrix for selective catalytic hydrogenation of nitroarenes, *J. Catal.* 357 (2018) 20–28.
- [59] F. Tang, G. Zhang, L. Wang, J. Huang, Y.-N. Liu, Unsymmetrically N, S-coordinated single-atom cobalt with electron redistribution for catalytic hydrogenation of quinolines, *J. Catal.* 414 (2022) 101–108.
- [60] H. Jasuja, K.S. Walton, Effect of catenation and basicity of pillared ligands on the water stability of MOFs, *Dalton Trans.* 42 (2013) 15421–15426.
- [61] F.S. Shirazi, K. Akhbari, Solid-state thermal conversion of a nanoporous metal-organic framework to a nonporous coordination polymer, *RSC Adv.* 5 (2015) 50778–50782.
- [62] D. Xu, R. Liu, J. Li, H. Zhao, J. Ma, Z. Dong, Atomically dispersed Co-N₄ sites anchored on N-doped carbon for aqueous phase transfer hydrogenation between nitroarenes and saturated N-heterocycles, *Appl. Catal. B Environ.* 299 (2021), 120681.
- [63] H. Xu, S. Zhang, J. Geng, G. Wang, H. Zhang, Cobalt single atom catalysts for the efficient electrosynthesis of hydrogen peroxide, *Inorg. Chem. Front.* 8 (2021) 2829–2834.
- [64] X. Wu, J.W. Sun, P.F. Liu, J.Y. Zhao, Y. Liu, L. Guo, S. Dai, H.G. Yang, H. Zhao, Molecularly dispersed cobalt phthalocyanine mediates selective and durable CO₂ reduction in a membrane flow cell, *Adv. Funct. Mater.* 32 (2022), 2107301.
- [65] J. Zang, F. Wang, Q. Cheng, G. Wang, L. Ma, C. Chen, L. Yang, Z. Zou, D. Xie, H. Yang, Cobalt/zinc dual-sites coordinated with nitrogen in nanofibers enabling efficient and durable oxygen reduction reaction in acidic fuel cell, *J. Mater. Chem. A* 8 (2020) 3686–3691.
- [66] X. Sun, A.I. Olivos-Suarez, D. Osadchii, M.J.V. Romero, F. Kapteijn, J. Gascon, Single cobalt sites in mesoporous N-doped carbon matrix for selective catalytic hydrogenation of nitroarenes, *J. Catal.* 357 (2018) 20–28.

- [67] Z. Teng, Q. Zhang, H. Yang, K. Kato, W. Yang, Y.-R. Lu, S. Liu, C. Wang, A. Yamakata, C. Su, B. Liu, T. Ohno, Atomically dispersed antimony on carbon nitride for the artificial photosynthesis of hydrogen peroxide, *Nat. Catal.* 4 (2021) 374–384.
- [68] L. Meng, E. Zhang, H. Peng, Y. Wang, D. Wang, H. Rong, J. Zhang, Bi/Zn dual single-atom catalysts for electroreduction of CO₂ to syngas, *ChemCatChem* 14 (2022), e202101801.
- [69] Y.J. Sa, S.O. Park, G.Y. Jung, T.J. Shin, H.Y. Jeong, S.K. Kwak, S.H. Joo, Heterogeneous Co-N/C electrocatalysts with controlled cobalt site densities for the hydrogen evolution reaction: structure-activity correlations and kinetic insights, *ACS Catal.* 9 (2019) 83–97.
- [70] X. Hai, X. Zhao, N. Guo, C. Yao, C. Chen, W. Liu, Y. Du, H. Yan, J. Li, Z. Chen, X. Li, Z. Li, H. Xu, P. Lyu, J. Zhang, M. Lin, C. Su, S.J. Pennycook, C. Zhang, S. Xi, J. Lu, Engineering local and global structures of single Co atoms for a superior oxygen reduction reaction, *ACS Catal.* 10 (2020) 5862–5870.
- [71] P. Christopher, Single-atom catalysts: are all sites created equal? *ACS Energy Lett.* 4 (2019) 2249–2250.
- [72] X. Wang, Z. Chen, X. Zhao, T. Yao, W. Chen, R. You, C. Zhao, G. Wu, J. Wang, W. Huang, J. Yang, X. Hong, S. Wei, Y. Wu, Y. Li, Regulation of coordination number over single co sites: triggering the efficient electroreduction of CO₂, *Angew. Chem. Int. Ed.* 57 (2018) 1944–1948.
- [73] R. Li, D. Wang, Understanding the structure-performance relationship of active sites at atomic scale, *Nano Res.* 15 (2022) 6888–6923.
- [74] Y. Huang, F. Rehman, M. Tamtaji, X. Li, Y. Huang, T. Zhang, Z. Luo, Mechanistic understanding and design of non-noble metal-based single-atom catalysts supported on two-dimensional materials for CO₂ electroreduction, *J. Mater. Chem. A* 10 (2022) 5813–5834.